Available online at www.sciencedirect.com
SCIENCE DIRECT®
Journal of Sound and Vibration 283 (2005) 765–779
JOURNAL OF SOUND AND VIBRATION
www.elsevier.com/locate/jsvi

Critical speeds of a spinning thin disk with an external ring

Anirvan DasGupta*, Peter Hagedorn

Institut für Mechanik, Technische Universität Darmstadt, 64289 Darmstadt, Germany

Received 28 April 2003; received in revised form 26 January 2004; accepted 13 May 2004
Available online 11 November 2004

Abstract

In this work, the dynamics of a spinning thin axisymmetric annular disk with an external ring have been studied and the effect of the ring on the critical speeds of the disk has been investigated. The disk with a ring is modelled using the von Karman plate theory and assuming clamped inner-boundary and free outer boundary. The self-adjoint eigenvalue problem for the linear stiffness operator is solved approximately using the Galerkin method to obtain the linear mode shapes and eigenvalues. These are then used to solve the eigenfrequencies of vibration of the disk. The spin speed corresponding to zero eigenfrequency of a particular mode is the critical speed for that mode. It has been shown that the critical speeds of the disk can be increased substantially by appropriate design of the external ring. A ring of uniform thickness is observed to reduce rather than increase the critical speeds. On the other hand, a tapered ring with increasing thickness is the outward radial direction can greatly improve the critical speeds. These observations have important implications for design of disks for high-speed applications as in computer hard-disk drives.

1. Introduction

High-speed spinning disks are found in various applications such as computer hard-disk drives, circular saws et cetera. With increasing speed, the stiffness of a particular mode of deflection of the disk tends to decrease leading to increase in vibration amplitude corresponding to that mode.

*Corresponding author. Presently at: Department of Mechanical Engineering, IIT Kharagpur, Kharagpur 721302, India.
E-mail address: anir@mech.iitkgp.ernet.in (A. DasGupta).

0022-460X/$ - see front matter © 2004 Published by Elsevier Ltd.
doi:10.1016/j.jsv.2004.05.019

Large-amplitude vibrations of the disk can produce undesirable effects and affect its performance. The critical speed, thus, limits the safe operating speed of the disk. For high-speed and high-precision applications, one of the possible ways to increase the operating speed is to improve the disk design to achieve high critical speeds.

The first attempt at understanding the classical linear vibrations of disks was made by Lamb and Southwell [1] in connection with vibrations of turbine disks. However, the non-linear dynamics of thin disks using the von Karman plate model was first investigated by Nowinski [2]. A study of the effect of transverse loading on the stability of spinning disks was carried out by Iwan and Moeller [3]. They studied the stability of single and multi-mode solutions of a linear model of the disk interacting with a stationary mass–spring–damper system and concluded that the disk system becomes unstable at super-critical speeds due to the effect of the spring. Further, the damper was found to make the disk unstable for all speeds above the lowest critical speed. Investigations on the effect of stationary transverse loads on spinning disks have also been reported in Refs. [4–6]. Shen and Mote [7] studied the mechanisms of instability of a circular plate parametrically exited by a rotating spring–mass–dashpot system. Similar conclusions as in Ref. [3] were drawn, and their phenomenological reasons were provided. Introduction of in-plane stresses using plastic deformation to increase the natural frequencies of circular saws was suggested by Mote [8]. The effect of edge beams on the natural frequencies and buckling loads of radially compressed annular plates was studied by Loh and Carney [9]. The idea of introducing membrane tensioning to suppress resonant behaviour was forwarded by Bension and Takahashi [10]. This idea was generated from the observation that the stress-free edge of the disk cannot resist the transverse deflection. However, their scheme requires a frame on which the membrane disk is tensioned. The idea of speed-dependent stressing of the inner periphery of a disk to raise its critical speed was proposed by Renshaw [11] and investigated further in Ref. [12]. Their method requires radially moving wedges to be installed on the inner edge of the disk to provide the necessary centrifugal stressing. Recently, Shen [13], in a review of research on rotating disks, has stressed on the importance of increasing the critical speeds of disks without increasing the thickness. In this direction, Renshaw [14] has proposed the use of internal channels in disks to raise the critical speeds. It is argued in Ref. [14] that the removal of material to make the channels will increase the natural frequency of the disk, while maintaining the coupling between the deflections of the upper and lower surfaces of the disk. About 10–100% improvement in the critical speeds were observed. However, this method requires the construction of dense internal channels in a thin disk which might be difficult in many cases. In another work, Renshaw [15] has suggested thickening of the clamped part of the disk to maximize the natural frequencies. Raman and Mote [16] have indicated that introduction of sufficiently high asymmetry in the disk can reduce the vibration energy near the critical rotation speeds. Their analysis may provide guidelines of designing circular saws and computer disks with imperfections to reduce the vibrations near the critical speed. Optimal thickness profile for maximizing critical speeds of rotating disks has been investigated by Warner and Renshaw [17]. However, the proposed method may be applicable only to circular saws.

In this work, we propose a new idea for improving the critical speeds of rotating thin disks without increasing the disk thickness. The idea consists of attaching a stiff ring of an appropriate width and varying thickness on the outer periphery of the disk. We model the composite system using the von Karman plate theory over the two fields of the disk and the ring with appropriate

interface and boundary conditions. It is assumed that the inner edge of the disk is perfectly clamped. The eigenfrequency calculation of the composite disk is simplified by first approximately solving a self-adjoined eigenvalue problem of the composite stiffness operator of the disk–ring system using the Galerkin method. This yields the mode shapes which are then used in the field equations of the disk and the ring to compute the eigenfrequencies of vibration. From the numerical calculations, it is shown that the critical speeds of the disk can be significantly improved by suitably tapering the external ring. A uniform ring is observed to reduce rather than increase the critical speeds. Any added mass at the periphery actually lowers the natural frequencies (as can be understood from the example of a cantilever with end mass). However, it is shown here that, in the case of disks, this increase of the peripheral mass due to the ring can be offset by increasing the stiffness through introduction of an appropriate radial taper. Numerical results for a polymer disk with an aluminium alloy ring and a steel ring have been obtained and compared.

2. Dynamics of a rotating disk with external ring

2.1. Equations of motion

Consider a symmetric annular disk of uniform thickness with an external ring of radially varying thickness as shown in Fig. 1. The thickness of the composite disk is assumed to be small and symmetric about a neutral plane which allows one to treat it as a plane stress problem. First, the equations of motion of a disk with varying thickness are derived, from which the uniform thickness case will follow. All the following derivations are performed in the inertial space.

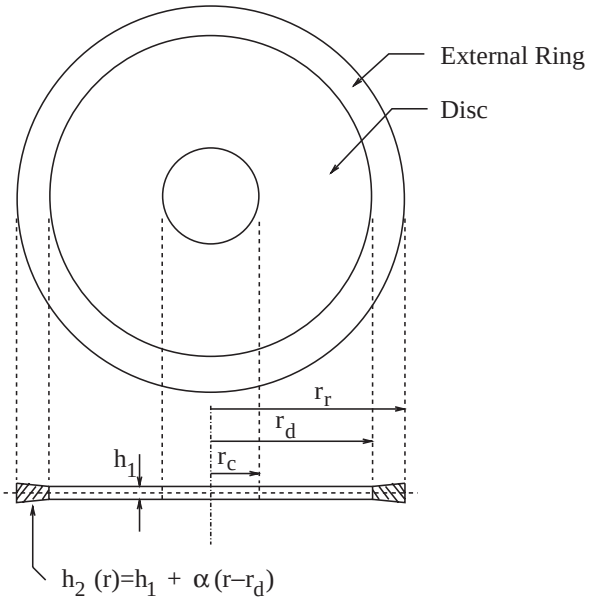

Fig. 1. Disk with an external ring.

Assume a cylindrical polar coordinate system at the centre of the disk with the r and θ axes lying on the neutral plane. The strains at any level z from the neural plane are obtained by substituting the classical plate deformation kinematic relations in the non-linear strain–displacement relations as (see Ref. [18])

$$\varepsilon_r = u^N_{,r} - z w^N_{,rr} + \tfrac{1}{2}(w^N_{,r})^2, \tag{1}$$

$$\varepsilon_\theta = \frac{u^N}{r} - \frac{z}{r}\, w^N_{,r} + \frac{1}{r}\, v^N_{,\theta} - \frac{z}{r^2}\, w^N_{,\theta\theta} + \frac{1}{2r^2}(w^N_{,\theta})^2, \tag{2}$$

$$\gamma_{r\theta} = \frac{1}{r} u^N_{,\theta} - \frac{2z}{r}\, w^N_{,r\theta} + v^N_{,r} + \frac{2z}{r^2}\, w^N_{,\theta} - \frac{v^N}{r} + \frac{1}{r}\, w^N_{,r} w^N_{,\theta}, \tag{3}$$

where ε_r and ε_θ are the normal strains along the r and θ directions, respectively, $\gamma_{r\theta}$ is the shear strain, u^N, v^N and w^N represent the displacements of a point on the neutral plane along r, θ and z directions, respectively, and the term(s) in the subscript after the comma implies (imply) partial derivative with respect to the indicated coordinate(s). Define the stress resultants

$$N_r = \int_{-h/2}^{h/2} \sigma_r \,\mathrm{d}z, \quad N_\theta = \int_{-h/2}^{h/2} \sigma_\theta \,\mathrm{d}z, \quad N_{r\theta} = \int_{-h/2}^{h/2} \tau_{r\theta} \,\mathrm{d}z, \tag{4}$$

$$M_r = \int_{-h/2}^{h/2} z\sigma_r \,\mathrm{d}z, \quad M_\theta = \int_{-h/2}^{h/2} z\sigma_\theta \,\mathrm{d}z, \quad M_{r\theta} = \int_{-h/2}^{h/2} z\tau_{r\theta} \,\mathrm{d}z, \tag{5}$$

$$Q_r = \int_{-h/2}^{h/2} \tau_{rz} \,\mathrm{d}z, \quad Q_\theta = \int_{-h/2}^{h/2} \tau_{\theta z} \,\mathrm{d}z, \tag{6}$$

where σ_r and σ_θ are the normal strains along the r and θ directions, respectively, $\tau_{r\theta}$ is the shear stress. It may be mentioned here that h may be an arbitrary function of r. Determining the stresses from Eqs. (1)–(3) using the Hooke's law and substituting into Eqs. (4) and (5) yields

$$N_r = h\sigma^N_r, \quad N_\theta = h\sigma^N_\theta, \quad N_{r\theta} = h\tau^N_{r\theta}, \tag{7}$$

$$M_r = -D^*\left[w^N_{,rr} + \frac{v}{r}\, w^N_{,r} + \frac{v}{r^2}\, w^N_{,\theta\theta}\right], \tag{8}$$

$$M_\theta = -D^*\left[v w^N_{,rr} + \frac{1}{r}\, w^N_{,r} + \frac{1}{r^2}\, w^N_{,\theta\theta}\right], \tag{9}$$

$$M_{r\theta} = -D^*\,\frac{1-v}{r}\left(w^N_{,r} - \frac{w^N}{r}\right)_\theta, \tag{10}$$

where $D^* = Eh^{*3}/[12(1-v^2)]$, E is Youngs' modulus, v is Poissons' ratio, and

$$\sigma^N_r = \frac{E}{1-v^2}\left[u^N_{,r} + \tfrac{1}{2}(w^N_{,r})^2 + v\left(\frac{u^N}{r} + \frac{v^N_{,\theta}}{r} + \frac{(w^N_{,\theta})^2}{2r^2}\right)\right], \tag{11}$$

$$\sigma_\theta^N = \frac{E}{1-\nu^2}\left[\nu\left(u_{,r}^N + \tfrac{1}{2}(w_{,r}^N)^2\right) + \frac{u^N}{r} + \frac{v_{,\theta}^N}{r} + \frac{(w_{,\theta}^N)^2}{2r^2}\right], \tag{12}$$

$$\tau_{r\theta}^N = \frac{E}{2(1+\nu)}\left[\frac{u_{,\theta}^N}{r} + v_{,r}^N - \frac{v^N}{r} + \frac{w_{,r}^N w_{,\theta}^N}{r}\right]. \tag{13}$$

Now, using Eqs. (7)–(10) and referring to Fig. 2, d'Alembert's principle yields the force and moment equilibrium relations as

$$\sigma_{r,r}^N + \frac{1}{r}\,\tau_{r\theta,\theta}^N + \frac{\sigma_r^N - \sigma_\theta^N}{r} + \rho^* r\omega^2 = 0, \tag{14}$$

$$\tau_{r\theta,r}^N + \frac{1}{r}\,\sigma_{\theta,\theta}^N + \frac{2\tau_{r\theta}^N}{r} = 0, \tag{15}$$

$$\rho^* h\,\frac{\mathrm{D}^2 w}{\mathrm{D}t^2} = \frac{Q_r}{r} + Q_{r,r} + \frac{Q_{\theta,\theta}}{r} + \frac{1}{r}[rh\sigma_r^N w_{,r}^N + h\tau_{r\theta}^N w_{,\theta}^N]_{,\,r} + \frac{1}{r}\left[h\tau_{r\theta}^N w_{,r}^N + \frac{h\sigma_\theta^N}{r}\,w_{,\theta}^N\right]_{,\theta}, \tag{16}$$

$$M_{r,r} + \frac{M_{r\theta,\theta}}{r} - \frac{M_\theta}{r} + \frac{M_r}{r} + Q_r = 0, \tag{17}$$

$$\frac{M_{r\theta,\theta}}{r} + \frac{2M_{r\theta}}{r} + M_{r\theta,r} + Q_\theta = 0, \tag{18}$$

where ρ^* is the density, ω is the magnitude of the angular velocity, and $\mathrm{D}(\cdot)/\mathrm{D}t$ represents the material derivative. It may be noted that the in-plane and rotary inertia of the element have been neglected. The in-plane force equilibrium relations (14) and (15) are identically satisfied by assuming a scalar stress function ϕ^* such that (see Ref. [19])

$$\sigma_r^N = \frac{\phi_{,r}^*}{r} + \frac{\phi_{,\theta\theta}^*}{r^2} - \tfrac{1}{2}\rho^* r^2\omega^2, \tag{19}$$

$$\sigma_\theta^N = \frac{\phi_{,r}^*}{r} - \tfrac{1}{2}\rho^* r^2\omega^2, \tag{20}$$

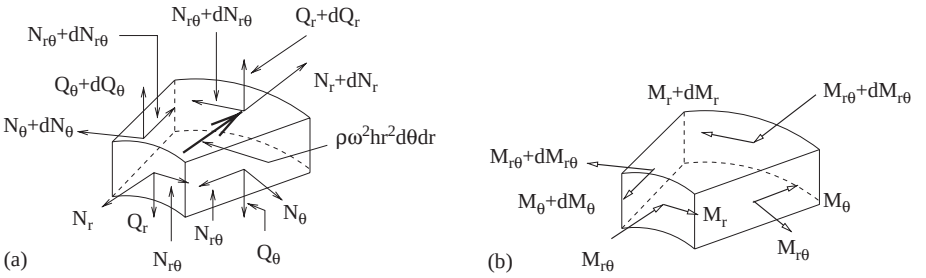

Fig. 2. Disk element with (a) forces, and (b) moments.

$$\tau_{r\theta}^{N} = -\left(\frac{\phi^*_{,\theta}}{r}\right)_{,r}. \tag{21}$$

Now, solving for Q_r and Q_θ using Eqs. (8)–(10) in Eqs. (17)–(18) and substituting into Eq. (16), and further using Eqs. (19)–(21), yields the equation of motion

$$\rho^* h(w^N_{,tt} + 2\omega w^N_{,\theta t} + \omega^2 w^N_{,\theta\theta}) + \nabla^2 D^* \nabla^2 w^N - (1-\nu)\mathscr{F}[w^N, D^*] - h\mathscr{F}[w^N, \phi^*]$$
$$+ \tfrac{1}{2}\rho^*\omega^2 r^2 h\nabla^2 w^N + \rho^*\omega^2 r h w^N_{,r} - h_{,r}\left[\left(\frac{\phi^*_{,r}}{r} + \frac{\phi^*_{,\theta\theta}}{r^2} - \tfrac{1}{2}\rho^*\omega^2 r^2\right)w^N_{,r} - \frac{1}{r}\left(\frac{\phi_{,\theta}}{r}\right)_{,r} w^N_{,\theta}\right] = 0, \tag{22}$$

where ∇^2 is the Laplacian operator, and

$$\mathscr{F}[X, Y] = X_{,rr}\left(\frac{Y_{,r}}{r} + \frac{Y_{,\theta\theta}}{r^2}\right) - 2\left(\frac{X_{,\theta}}{r}\right)_{,r}\left(\frac{Y_{,\theta}}{r}\right)_{,r} + Y_{,rr}\left(\frac{X_{,r}}{r} + \frac{X_{,\theta\theta}}{r^2}\right). \tag{23}$$

The stress function ϕ^* can be expressed in terms of the deflection w^N by eliminating u^N and v^N from Eqs. (11)–(13) and (19)–(21) as

$$\nabla^4\phi^* = -\tfrac{1}{2}E\mathscr{F}[w^N, w^N] + 2(1-\nu)\rho^*\omega^2. \tag{24}$$

Therefore, the equations of motion of the composite disk can now be written in non-dimensional form using the following definitions:

$$u_i = u_i^N/h_1^*, \quad v_i = v_i^N/h_1^*, \quad w_i = w_i^N/h_1^*,$$
$$\tilde{r} = r/r_d, \quad \tilde{t} = t\sqrt{\frac{D_1^*}{hr_d^4\rho_1}}, \quad \Omega = \omega\sqrt{\frac{hr_d^4\rho_1}{D_1^*}},$$
$$\phi_i = \phi_i^*\,\frac{h_1^*}{D_1^*} \quad h = \frac{h_2^*}{h_1^*}, \quad D = \frac{D_2^*}{D_1^*}, \quad \rho = \frac{\rho_2^*}{\rho_1^*},$$
$$\tilde{r}_c = \frac{r_c}{r_d}, \quad \tilde{r}_d = 1, \quad \tilde{r}_r = \frac{r_r}{r_d}, \tag{25}$$

as

$\tilde{r}_c \leqslant \tilde{r} \leqslant \tilde{r}_d$:

$$w_{1,\tilde{t}t} + 2\Omega w_{1,\theta\tilde{t}} + \Omega^2 w_{1,\theta\theta} + \nabla^4 w_1 - \mathscr{F}[w_1, \phi_1] + \tfrac{1}{2}\Omega^2\tilde{r}^2\nabla^2 w_1 + \Omega^2\tilde{r}w_{1,\tilde{r}} = 0, \tag{26}$$

$$\nabla^4\phi_1 = -6(1-\nu_1^2)\mathscr{F}[w_1, w_1] + 2(1-\nu_1)\Omega^2, \tag{27}$$

$\tilde{r}_d < \tilde{r} \leqslant \tilde{r}_r$:

$$\rho h(w_{2,\tilde{t}t} + 2\Omega w_{2,\theta\tilde{t}} + \Omega^2 w_{2,\theta\theta}) + \nabla^2 D\nabla^2 w_2 - (1-\nu_2)\mathscr{F}[w_2, D] - h\mathscr{F}[w_2, \phi_2]$$
$$+ \rho h\left(\tfrac{1}{2}\Omega^2\tilde{r}^2\nabla^2 w_2 + \Omega^2\tilde{r}w_{2,\tilde{r}}\right)$$
$$- h_{,\tilde{r}}\left[\left(\frac{\phi_{2,\tilde{r}}}{r} + \frac{\phi_{2,\theta\theta}}{\tilde{r}^2} - \tfrac{1}{2}\rho\Omega^2\tilde{r}^2\right)w_{2,\tilde{r}} - \frac{1}{\tilde{r}}\left(\frac{\phi_{2,\theta}}{\tilde{r}}\right)_{,\tilde{r}} w_{2,\theta}\right] = 0, \tag{28}$$

$$\nabla^4\phi_2 = -6(1-\nu_2^2)\left(\frac{E_2}{E_1}\right)\mathscr{F}[w_2, w_2] + 2(1-\nu_2)\Omega^2, \tag{29}$$

where $i = 1$ represents the disk, and $i = 2$ corresponds to the ring. In the following, the tilde symbol will be dropped for convenience.

2.2. Boundary conditions

The boundary conditions for the composite disk are as follows:

$$r = r_c \quad \text{and} \quad \theta \in [0, 2\pi]:$$

$$w_1 = 0, \quad w_{1,r} = 0, \tag{30}$$

$$u_1 = 0, \quad v_1 = 0, \tag{31}$$

$$r = r_d \quad \text{and} \quad \theta \in [0, 2\pi]:$$

$$w_2 = w_1, \quad w_{2,r} = w_{1,r}, \tag{32}$$

$$u_2 = u_1, \quad v_2 = v_1, \tag{33}$$

$$\sigma_{r1}^N = \sigma_{r2}^N, \quad \tau_{r\theta 1}^N = \tau_{r\theta 2}^N, \tag{34}$$

$$-\left[w_{1,rr} + \frac{\nu_1}{r}\, w_{1,r} + \frac{\nu_1}{r^2}\, w_{1,\theta\theta}\right] = -D\left[w_{2,rr} + \frac{\nu_2}{r}\, w_{2,r} + \frac{\nu_2}{r^2}\, w_{2,\theta\theta}\right], \tag{35}$$

$$\begin{aligned} &-\left[\frac{1-\nu_1}{r^2}\left(w_{1,r} - \frac{w_1}{r}\right)_{,\theta\theta} + (\nabla^2 w_1)_{,r}\right] \\ &= -D\left[\frac{1-\nu_2}{r^2}\left(w_{2,r} - \frac{w_2}{r}\right)_{,\theta\theta} + (\nabla^2 w_2)_{,r}\right] - D_{,r}\left[w_{2,rr} + \frac{\nu_2}{r}\, w_{2,r} + \frac{\nu_2}{r^2}\, w_{2,\theta\theta}\right]. \end{aligned} \tag{36}$$

$$r = r_r \quad \text{and} \quad \theta \in [0, 2\pi]:$$

$$\sigma_{r2}^N = 0, \quad \tau_{r\theta 2}^N = 0, \tag{37}$$

$$\left[w_{2,rr} + \frac{\nu_2}{r}\, w_{2,r} + \frac{\nu_2}{r^2}\, w_{2,\theta\theta}\right] = 0, \tag{38}$$

$$-D\left[\frac{1-\nu_2}{r^2}\left(w_{2,r} - \frac{w_2}{R}\right)_{,\theta\theta} + (\nabla^2 w_2)_{,r}\right] - D_{,r}\left[w_{2,rr} + \frac{\nu_2}{r}\, w_{2,r} + \frac{\nu_2}{r^2}\, w_{2,\theta\theta}\right] = 0. \tag{39}$$

Thus, Eqs. (26)–(29) along with the boundary conditions (30)–(39) represent the complete dynamics of the axisymmetric clamped–free annular disk with an external ring of radially varying thickness. It may be noted that the equations of motion (26)–(29) are non-linear. However, for the present analysis of critical speeds, only the linear dynamics will be relevant. It can be easily observed that the linear dynamics is obtained by dropping the non-linear terms $\mathscr{F}[w_1, w_1]$ and $\mathscr{F}[w_2, w_2]$ in the stress function equations (27) and (29), respectively.

2.3. Solution of stress function equations

Dropping the non-linear terms in Eqs. (27) and (29) allows one to solve them in closed form as follows. Assume a solution of the stress function $\phi_i = \phi_{ih} + \phi_{ip},\ i = 1, 2$, such that

$$\nabla^4 \phi_{ih} = 0, \tag{40}$$

and

$$\nabla^4 \phi_{ip} = 2(1 - \nu_i)\Omega^2. \tag{41}$$

Then, the solutions can be written as (see Ref. [20])

$$\phi_{ih} = \delta_{i0} \ln r + \delta_{i1} r^2 + \delta_{i2} r^2 \ln r, \tag{42}$$

$$\phi_{ip} = \frac{1 - \nu_i}{32} \Omega^2 r^4, \tag{43}$$

where the six δ_{ij}s are the constants of integration to be determined using the boundary conditions (31), (33), (34), (37). It may be observed that the second boundary condition in Eqs. (34) and (37) are identically satisfied since the solutions (42) and (43) are independent of θ. That leaves only six boundary conditions from which the six unknowns can be solved.

3. Galerkin method and complex normal modes of vibration

In order to simplify the dynamics represented by Eqs. (26)–(29) and calculate the critical speeds, a two-step procedure is adopted. First, the eigenvalue problem of a self-adjoint composite stiffness operator of the disk–ring system is solved yielding the mode shapes of the disk. Next, the eigenfrequency of any particular mode is computed using its mode shape solution (obtained from the previous step) in the complete field equation of the disk–ring system. In both the above steps, the Galerkin method is used. The procedure described above is now detailed in the following.

Define the two stiffness operators over the disk and the ring, respectively, as

$$\mathscr{L}_1(w_1) = \nabla^4 w_1 - \mathscr{F}[w_1, \phi_1] + \frac{1}{2} \Omega^2 r^2 \nabla^2 w_1 + \Omega^2 r w_{1,r}, \tag{44}$$

$$\begin{aligned}\mathscr{L}_2(w_2) = {} & \nabla^2 D \nabla^2 w_2 - (1 - \nu_2)\mathscr{F}[w_2, D] - h\mathscr{F}[w_2, \phi_2] \\ & + \rho h \left(\tfrac{1}{2} \Omega^2 r^2 \nabla^2 w_2 + \Omega^2 r w_{2,r} \right) - h_{,r} \left[\left(\frac{\phi_{2,r}}{r} + \frac{\phi_{2,\theta\theta}}{r^2} - \frac{1}{2} \rho \Omega^2 r^2 \right) w_{2,r} - \frac{1}{r} \left(\frac{\phi_{2,\theta}}{r} \right)_{,r} w_{2,\theta} \right].\end{aligned} \tag{45}$$

Let a composite stiffness operator over the whole domain of the disk–ring system be represented by $\mathscr{L}_1 \oplus \mathscr{L}_2(w_1 \oplus w_2) = \mathscr{L}_1(w_1) \oplus \mathscr{L}_2(w_2)$, where $w_1 \oplus w_2$ is an element of the composite displacement field consisting of the disk and the ring. Then the following eigenvalue problem may be defined

$$\mathscr{L}_1 \oplus \mathscr{L}_2(w_1 \oplus w_2) = \lambda^2 w_1 \oplus \rho h w_2. \tag{46}$$

Over the composite displacement field, we define the following inner product:

$$\langle w_{11} \oplus w_{12}, w_{21} \oplus w_{22} \rangle = \int_0^{2\pi} \int_{r_c}^{r_d} \bar{w}_{11} w_{21} r \, \mathrm{d}\theta \, \mathrm{d}r + \int_0^{2\pi} \int_{r_d}^{r_r} \bar{w}_{12} w_{22} r \, \mathrm{d}\theta \, \mathrm{d}r, \tag{47}$$

where $w_{11} \oplus w_{12}$ and $w_{21} \oplus w_{22}$ are any two elements of the composite displacement field, and the overbar implies complex conjugate.

The eigenvalue problem (46) is now solved using the Galerkin method. The periodicity in the θ direction allows one to assume an eigensolution of the form

$$w_1 \oplus w_2 = (P_{n1}(r) \oplus P_{n2}(r)) \mathrm{e}^{\mathrm{i}n\theta}, \tag{48}$$

which represents the nth complex mode shape, and n is the number of nodal diameters. It is convenient to express $P_{ni}(r)$ as linear combination of certain basis functions as $P_{ni}(r) = \sum_{j=0}^{M} k_j \psi_{ij}(r)$, where k_j are unknown constants, and $\psi_{ij}(r)$ are assumed basis functions for the mode shape which are assumed to satisfy all the boundary conditions (30) and (32), (35), (36), (38) and (39). A procedure of obtaining the basis functions is outlined in the Appendix. Now substituting Eq. (48) into the eigenvalue problem (46) and equating the projection of the residue along each basis function to zero using Eq. (47) yields

$$[B_{ij} - \lambda^2 C_{ij}]\mathbf{k} = 0, \tag{49}$$

where $B_{ij} = \langle \psi_{1i}(r) \oplus \psi_{2i}(r), \ \mathscr{L}_1 \oplus \mathscr{L}_2(\psi_{1j}(r) \oplus \psi_{2j}(r)) \rangle$, and $C_{ij} = \langle \psi_{1i}(r) \oplus \psi_{2i}(r), \psi_{1j}(r) \oplus \rho h \psi_{2j}(r) \rangle$ are both symmetric $M \times M$ matrices. For nontrivial solution of $\mathbf{k}$, we equate the determinant of the matrix in Eq. (49) to zero and solve for the M eigenvalues λ of the stiffness operator. The corresponding eigenvectors yield the mode shapes (eigenmodes). It may be mentioned that the different eigenvalues for any n correspond to different nodal circles, and the lowest eigenvalue corresponds to zero nodal circle. In further analysis, we consider only the zero nodal circle case since it is the lowest mode which is exited for any n. It may be noted that λ is a function of the angular velocity Ω.

Now, a harmonic solution (eigensolution) of Eqs. (26) and (28) is assumed having the form (see Ref. [16])

$$(w_1, w_2)^{\mathrm{T}} = a_n[(P_{n1}(r), P_{n2}(r))^{\mathrm{T}} \mathrm{e}^{\mathrm{i}n\theta}] \mathrm{e}^{\mu_n t} + \bar{a}_n[(P_{n1}(r), P_{n2}(r))^{\mathrm{T}} \mathrm{e}^{-\mathrm{i}n\theta}] \mathrm{e}^{\bar{\mu}_n t}, \tag{50}$$

where T in the superscript implies transpose, and a_n is a complex constant. Substituting solution (50) for zero nodal circle into the equations of motion (26) and (28) yields the residues

$$\mathrm{Res}_1 = a_n[\mathrm{e}^{\mathrm{i}n\theta}(\mu^2 + 2\mathrm{i}n\Omega\mu - n^2\Omega^2)P_{n1}(r) + \mathscr{L}_{1n}(P_{n1}(r))] \mathrm{e}^{\mathrm{i}n\theta + \mu t} + \text{c.c.}, \tag{51}$$

$$\mathrm{Res}_2 = a_n[\mathrm{e}^{\mathrm{i}n\theta}(\mu^2 + 2\mathrm{i}n\Omega\mu - n^2\Omega^2)P_{n2}(r) + \mathscr{L}_{2n}(P_{n2}(r))] \mathrm{e}^{\mathrm{i}n\theta + \mu t} + \text{c.c.}, \tag{52}$$

where c.c. denotes complex conjugate of the preceding expression, and $\mathscr{L}_{in}(\cdot)$ is such that $\mathscr{L}_i(P_{ni}(r)\mathrm{e}^{\mathrm{i}n\theta}) = \mathrm{e}^{\mathrm{i}n\theta}\mathscr{L}_{in}(P_{ni}(r))$. Using Eq. (47) to project the composite residue along the assumed eigenmode, and equating it to zero yields

$$\langle (P_{n1}(r) \oplus P_{n2}(r)) \mathrm{e}^{\mathrm{i}n\theta}, \mathrm{Res}_1 \oplus \mathrm{Res}_2 \rangle = 0 \tag{53}$$

or,

$$\left(\int_{r_c}^{r_d} P_{n1}^2(r)\,\mathrm{d}r + \rho\int_{r_d}^{r_r} hP_{n2}^2(r)\,\mathrm{d}r\right)(\mu^2 + 2\mathrm{i}n\Omega - n^2\Omega^2 + \lambda^2) = 0, \tag{54}$$

$$\Rightarrow \mu^2 + 2\mathrm{i}n\Omega - n^2\Omega^2 + \lambda^2 = 0, \tag{55}$$

where Eq. (54) is obtained from Eq. (53) using Eq. (49). Thus, Eq. (55) yields the eigenfrequencies of vibrations as $\mu_{\pm} = \mathrm{i}(-n\Omega \pm \lambda(\Omega))$. Angular speed Ω for which $\mu_{+} = 0$ is the critical speed for the corresponding mode. At the critical speed, the backward travelling wave will appear stationary in the inertial frame since its phase velocity goes to zero.

4. Numerical results and discussions

In this section, we present the numerical results of three cases, namely (a) disk without a ring, (b) disk with a uniform ring, and (c) disk with a tapering ring. The disk is assumed to be made of polymer, while the ring is made of an aluminium alloy. The various parameters of the disk and ring are taken as follows.

Disk parameters: $r_c = 0.015\,\mathrm{m}$, $r_d = 0.05\,\mathrm{m}$, $h_1^* = 0.001\,\mathrm{m}$,

$\rho_1^* = 2700\,\mathrm{kg/m^3}$, $E_1 = 40\,\mathrm{GPa}$, $v_1 = 0.25$.

Ring parameters: $r_r = 0.0525\,\mathrm{m}$, $h_2^* = 0.001 + \alpha(r - r_d)\,\mathrm{m}$,

$\rho_2^* = 3000\,\mathrm{kg/m^3}$, $E_2 = 80\,\mathrm{GPa}$, $v_2 = 0.33$,

where α represents the slope of the taper. The number of terms taken in the mode shape expansion, N (see the Appendix), was five. It was found that a five term expansion was enough to obtain a convergence in the non-dimensional critical speeds upto the first place of decimal. A high-strength aluminium alloy was taken as the ring material. Later, a comparison with a steel ring is also presented.

The non-dimensional frequency–speed diagram of the disk alone is shown in Fig. 3, where F and B, respectively, refer to the forward and backward wave frequencies. It is observed that the mode with one nodal diameter does not have a critical speed as proved in Ref. [21]. Further, the critical speed of the third mode (mode with three nodal diameters) is lower than that of the second mode. Next, we study the effect of α (the slope of the taper) and width of the ring on the critical speeds. In Figs. 4 and 5, the variation of the non-dimensional critical speed of the second and third mode, respectively, versus the ring width, for different values of α are presented. It is observed from Fig. 4 for the second mode that, for the uniform ring (i.e., $\alpha = 0$), the critical speed reduces. While, for non-zero values of α, the critical speed first reduces slightly and then increases. This is because, beyond a certain width of the ring, the increase in the section modulus (and hence

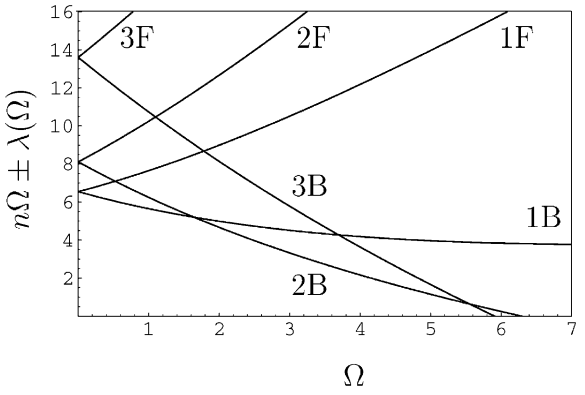

Fig. 3. Frequency–speed characteristics (F: forward wave; B: backward wave).

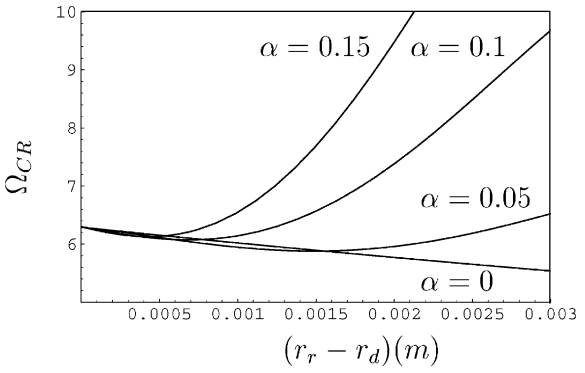

Fig. 4. Variation of critical speed of the second mode with ring width.

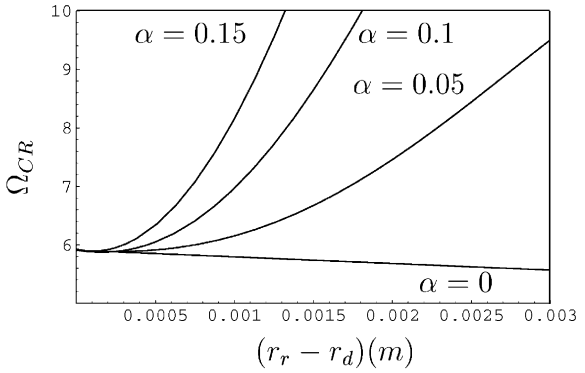

Fig. 5. Variation of critical speed of the third mode with ring width.

the stiffness) due to the taper outweighs the reduction in the critical speed due to increase in the radius of the disk and increase in the mass at the periphery. Similar trend is observed for the third mode in Fig. 5. Taking this observation into account, in the following, we consider only disk with tapered ring with $\alpha = 0.15$ unless mentioned otherwise.

Figs. 6 and 7, respectively, compare the non-dimensional eigenfrequency of the second mode and third mode of a normal disk against a disk with a tapered ring having $r_r = 0.0525\,\mathrm{m}$. Centrifugal stiffning causes the eigenfrequencies to increase as observed. The corresponding critical speeds are obtained from the intersection points of the curves with the lines 2Ω and 3Ω as shown in Figs. 6 and 7, respectively. Thus, for example in Fig. 6, the abscissa corresponding to X_{2d} is the critical speed of the second mode of the disk without the ring, while the abscissa of X_{2r} gives the corresponding critical speed of the disk with the ring. It is observed from the figures that a considerable increase in the critical speeds has been achieved. The numerical values of the critical speeds of the second and third modes without and with the ring are compared in Table 1. Thus, it is clear that the radial thickness variation of the ring has to be appropriate in order to achieve increased critical speeds of the disk. Fig. 8 presents the variation of the radial and hoop stress in the disk rotating at $\Omega = 4.0$. It is observed that the radial stress matches at the interface of

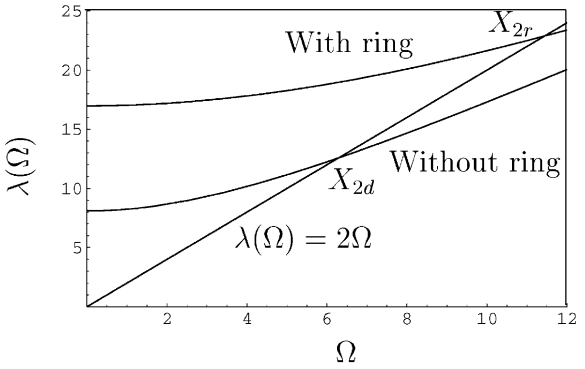

Fig. 6. Frequency variation of second mode with rotation speed (with ring: $\alpha = 0.15$, $r_r - r_d = 0.0025\,\mathrm{m}$).

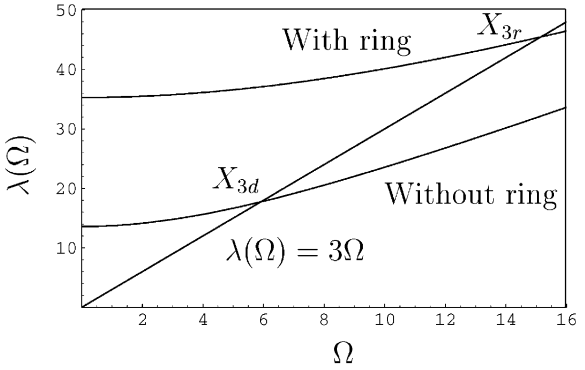

Fig. 7. Frequency variation of third mode with rotation speed (with ring: $\alpha = 0.15$, $r_r - r_d = 0.0025\,\mathrm{m}$).

Table 1
Critical speeds of second and third modes of disk without and with external ring

Mode number, n	Ω_{CR} (ω_{CR} RPM) (without ring)	Ω_{CR} (ω_{CR} RPM) (with ring)
2	6.2876 (27560.6)	11.4368 (50131.2)
3	5.90513 (25884.1)	15.1529 (66420.0)

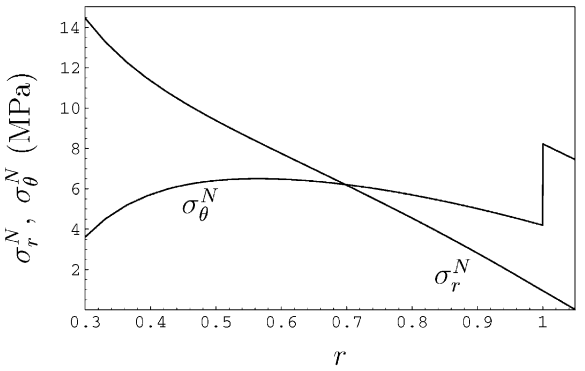

Fig. 8. Radial and hoop stresses in the disk and ring.

Table 2
Comparison of critical speeds of second and third modes of disk without, with uniform and with tapered external ring made of steel and aluminium

Mode number, n	Ω_{CR} (ω_{CR} RPM) (without ring)	Ω_{CR} (ω_{CR} RPM) (with uniform ring)		Ω_{CR} (ω_{CR} RPM) (with tapered ring)	
		Steel	Aluminium	Steel	Aluminium
2	6.2876 (27560.6)	5.0638 (22196.3)	5.65241 (24776.3)	11.9342 (52311.4)	11.4368 (50131.2)
3	5.90513 (25884.1)	5.34906 (23446.6)	5.62515 (24656.8)	20.9024 (91621.9)	15.1529 (66420.0)

the disk and the ring, and goes to zero at the outer periphery as expected. However, the hoop stress has a discontinuity at the disk–ring interface and is tensile. The high tensile hoop stress at the outer edge is one of the necessary features for increasing the critical speeds of disks as observed in Ref. [11]. However, the limit on the actual achievable speed will be decided by the ultimate strength of the disk and the ring materials.

To see the effect of change of material properties of the ring on the critical speeds, an example with a steel ring is compared with the results obtained above. For the steel ring, the following parameters are assumed: $\rho_2 = 7800\,\mathrm{kg/m^3}$, $E_2 = 190\,\mathrm{GPa}$, while the remaining parameters are kept unchanged. Table 2 compares the critical speeds for modes 2 and 3 with both, a uniform ring,

and a tapered ring with $\alpha = 0.15$. It may be observed that, for the uniform ring, the high density of steel (and hence high peripheral mass) actually reduces the critical speeds as was mentioned earlier. However, the introduction of the taper could significantly increase them even more than those achieved by the aluminium alloy ring.

5. Conclusions

In this study, a new idea for increasing the critical speeds of rotating thin disks has been examined. The idea is to attach a ring of appropriate variable thickness on the outer free edge of the disk. It has been shown that considerable improvement in the critical speeds can be achieved by appropriately designing the ring. The idea may also be extended to other applications such as circular saws in which the stiffning ring may be attached near the periphery. Another interesting extension of the present idea will be to study the effect of pre-stressing of the ring on the stability of the composite disk. The effect of channeling in the ring, as suggested in Ref. [14], can be another possible direction of further investigation.

Acknowledgements

The first author would like to gratefully acknowledge the financial support received by him from the Alexander von Humboldt-Foundation which made his stay and research in Germany possible.

Appendix A

A particular choice of the basis functions for the present problem may be written as

$$\tilde{\psi}_{1j}(r) = \sum_{k=0}^{N} b_{1k}(r - r_c)^{2+k}, \tag{A.1}$$

and

$$\tilde{\psi}_{2j}(r) = \sum_{k=0}^{N} b_{2k}(r - r_d)^{2+k} - \sum_{k=0}^{N} b_{1k}(r_d - r_c)^{2+k}, \tag{A.2}$$

or, in a compact form, as $(\tilde{\psi}_{1j}(r), \tilde{\psi}_{2j}(r))^{\mathrm{T}} = \mathbf{B}(r)\mathbf{x}$, where $\mathbf{B}(r)$ is a $2 \times 2N$ matrix, and $\mathbf{x}$ is a $2N \times 1$ vector of the coefficients b_{ij}s. Such a choice clearly satisfies the geometric boundary conditions (30) and (32). Substituting the eigensolution form (48) in the boundary conditions (35), (36), (38) and (39) yields four boundary condition equations in $2N$ unknowns b_{ij}s of the form $\mathbf{A}\mathbf{x} = 0$, where $\mathbf{A}$ is a constant $4 \times 2N$ matrix. Here it will be assumed that $N \gg 2$ so that there are many more unknowns than the number of equations. Thus, the solution of the boundary condition equations is of the form $\mathbf{x} = \mathbf{N}_{\mathbf{A}}\mathbf{k}$, where $\mathbf{N}_{\mathbf{A}}$ is a $2N \times (2N - 4)$ matrix such that its columns completely span the null space of $\mathbf{A}$, and $\mathbf{k}$ is an arbitrary $(2N - 4) \times 1$ vector. Then, $P_{ni}(r)$ in Eq. (48) can be

written as

$$P_{ni}(r) = \sum_{j=0}^{2N} k_j \psi_{ij}(r), \tag{A.3}$$

where $(\psi_{1j}(r), \psi_{2j}(r))^{\mathrm{T}} = \mathbf{B}(r)\mathbf{n}_{\mathbf{A}j}$, and $\mathbf{n}_{\mathbf{A}j}$ is the jth column of $\mathbf{N}_{\mathbf{A}}$.

References

[1] H. Lamb, R.V. Southwell, The vibrations of a spinning disc, *Proceedings of Royal Society, Series A* 99 (1921) 272–280.

[2] J.L. Nowinski, Nonlinear transverse vibrations of a spinning disc, *Journal of Applied Mechanics* 31 (1964) 72–78.

[3] W.D. Iwan, T.L. Moeller, The stability of a spinning elastic disk with transverse load system, *Journal of Applied Mechanics* 43 (1976) 485–490.

[4] H.J. Greenberg, Flexible disc—read/write head interface, *IEEE Transactions on Magnetics* MAG-14 (5) (1978) 336–338.

[5] R.C. Benson, D.B. Bogy, Deflection of a very flexible spinning disk due to a stationary transverse load, *Journal of Applied Mechanics* 45 (1978) 636–642.

[6] G.G. Adams, Analysis of the flexible disc/head interface, *Journal of Lubrication Techniques* 102 (1980) 86–90.

[7] I.Y. Shen, C.D. Mote Jr., On the mechanism of instability of a circular plate under a rotating spring–mass–dashpot system, *Journal of Sound and Vibration* 148 (2) (1991) 307–318.

[8] C.D. Mote Jr., Free vibration of initially stressed circular discs, *Journal of Engineering for Industry* 87 (1965) 258–264.

[9] H.C. Loh, J.F. Carney III, Vibration and stability of spinning annular plates reinforced with edge beams, *Journal of Applied Mechanics* 44 (1977) 499–501.

[10] R.C. Benson, T.T. Takahashi, Mechanics of flexible disks in magnetic recording, *Advances in Information Storage Systems* 1 (1991) 15–35.

[11] A.A. Renshaw, Increasing the maximum stable rotation speed of a circular disk using speed dependent clamping, *Journal of Sound and Vibration* 210 (1998) 431–439.

[12] H.R. Kim, A.A. Renshaw, Asymmetric speed dependent tensioning of circular rotating disks, *Journal of Sound and Vibration* 218 (1998) 65–72.

[13] I.Y. Shen, Vibration of flexible rotating disks, *The Shock and Vibration Digest* 32 (4) (2000) 267–272.

[14] A.A. Renshaw, Increasing the natural frequencies of circular disks using internal channels, *Journal of Sound and Vibration* 229 (2) (2000) 355–375.

[15] A.A. Renshaw, Maximizing the natural frequencies and transverse stiffness of centrally clamped, circular disks by thickening the clamped part of the disk, *Journal of Applied Mechanics* 66 (1999) 1017–1021.

[16] A. Raman, C.D. Mote Jr., Effects of imperfection on the non-linear oscillations of circular plates spinning near critical speed, *International Journal of Non-linear Mechanics* 36 (2001) 261–289.

[17] G.M. Warner, A.A. Renshaw, Thickness profiles for rotating circular disks that maximize critical speed, *Journal of Applied Mechanics* 68 (2001) 505–507.

[18] L.D. Landau, E.M. Lifshitz, *Theory of Elasticity*, Pergamon Press, Oxford, 1959.

[19] S. Timoshenko, J.N. Goodier, *Theory of Elasticity*, McGraw-Hill, New York, 1951.

[20] J.P. Den Hartog, *Advanced Strength of Materials*, McGraw-Hill, New York, 1952.

[21] A.A. Renshaw, C.D. Mote Jr., Absence of one nodal diameter critical speed modes in an axisymmetric rotating disc, *Journal of Applied Mechanics* 59 (1992) 687–688.